RSC Advances

ROYAL SOCIETY OF CHEMISTRY

www.rsc.org/advances

Journal Name

ARTICLE

QM/MD simulations on the role of SiO_2 in polymeric insulation materials

Received 00th January 20xx,
Accepted 00th January 20xx

DOI: 10.1039/x0xx00000x

www.rsc.org/

Baozhong Han,[a,c] Menggai Jiao,[b] Chengcheng Zhang,[a] Chunyang Li,[a] Zhijian Wu,[b] Ying Wang*[a,b] and Hui Zhang*[a]

Quantum chemical molecular dynamics (QM/MD) simulations based on self-consistent charge density functional tight-binding (SCC-DFTB) method on SiO_2 filling in the polyethylene (PE) showed that: in the absence of SiO_2, the PE was quickly charged by the high-energy electrons, which resulted in C-C or C-H bonds breaking; On the contrary, in the presence of SiO_2 nanoclusters, electrons trapping and accumulating were dominated by SiO_2 nanoclusters rather than polyethylene, which made polyethylene be preferentially protected and the initial time of electrical treeing increased. In our calculations, we also observed the double electric layers around the SiO_2 nanocluster, in agreement with recent suggestions from experiments. Furthermore, compared with some other investigated nanoclusters, SiO_2 was regarded as the most promising candidate attributing to the highest electron affinity. We further observed that once the high-energy electrons were supersaturated in the nanoclusters, the polyethylene chains would be unavoidably charged and C-H bonds breaking occurred, which resulted from the interaction between H and O or Si in the nanoclusters. Following that the polyethylene chains decomposing and cross-linking were involved into the initial growth of electrical treeing. The current observation can be potentially used in power cable insulation.

Introduction

Nowadays, polymeric insulation materials, such as cross-linked polyethylene (XLPE), are widely used in high voltage equipment due to the superiority of electrical performance. However, it is unavoidable that the polymeric materials will be aged and finally results in dielectric breakdown. The main reason of dielectric breakdown is attributed to electrical treeing.[1] Significant efforts have been dedicated towards understanding the electrical treeing mechanism and inhibiting the electrical treeing formation. Numerous researches have predicted that filling nano-sized particles, such as SiO_2,[2-6] MgO,[7,8] ZnO,[9-11] Al_2O_3,[12] TiO_2,[13] C_{60},[14-17] and PCBM ([6,6]-phenyl-C_{61}-butyric acid methyl ester),[17,18] was a very promising method in improving the electrical tree resistance and may considerably enhance the transmission efficiency of power grids. Basically, tree initial voltage, tree breakdown voltage, tree initial time, and tree breakdown time are four parameters that have been used to investigate the effectiveness and capabilities of filler to suppress the growth of electrical treeing. Experiments[2-6] have found that silica nanofiller prolonged the tree initiation time and increased the tree breakdown voltage; filling MgO[7,8] or TiO_2[13] nanoparticles could increase the tree breakdown time or increase the tree growth time.

Currently, the essential role of nano-composites was explained in the following aspects: The main advantage of filling nano-sized particles was to provide the larger surface area, which is related to interfacial region of filler and polymer;[19] another superiority is the surface interaction between polymer and nanoparticles affect the electrical properties of the dielectric material.[20] Generally, the behaviour of nanocomposite material is dominated by the properties of the interfaces of nanoparticles with its surrounding environment. The interfacial region addition of nanoparticles in polymer matrix can change some of the structural properties such as local charge, local conductivity distribution, free volume, and charge mobility; also, the charge carriers could be trapped much easier by nanoparticles and these additives could scavenge high-energy electrons, which reduced the accumulated damage in the material and avoided the degradation of polyethylene chains,[21] thereby increasing the life time of the polymer. Moreover, by collision with the nanoparticles, the high-energy electrons will lose energy and result in the reduction of treeing; nanoparticle can also be responsible for the stability of PE since the PE chains are strongly attracted by the nanoparticle surfaces.

Although the presence of nanoparticles or nanoclusters in polymer matrix hindering the electrical tree propagation has been widely observed in the experiments, the essence of the

[a] Key Laboratory of Engineering Dielectrics and Its Application (Harbin University of Science and Technology), Ministry of Education, Harbin, 150080, PR China. Email: huizhang@hrbust.edu.cn
[b] State Key Laboratory of Rare Earth Resource Utilization, Changchun Institute of Applied Chemistry, Chinese Academy of Sciences, Changchun 130022, PR China. Email: ywang_2012@ciac.ac.cn
[c] Shanghai Qifan Wire Admdcable Co., LTD., Shanghai 200008, PR China.
† Electronic Supplementary Information (ESI) available: The last snapshots at 60ps for each trajectory,The RDF of Mulliken charge distribution and the Lindemann Index for individual trajectory. See DOI: 10.1039/x0xx00000x

obstacle effect is still not clear. Therefore, further researches on electrical treeing and its formation mechanism in nanocomposites are urgently required. In this paper, by quantum chemical molecular dynamics (QM/MD) simulations we focused on the effect of SiO_2 nanoclusters on charge redistribution and electrons trapping, and investigated the role of SiO_2 as voltage stabilizers for high-voltage power cable insulation. Furthermore, we discussed the interaction between nanocluster and polyethylene to explain the critical effect of interfacial region. The current observation can potentially be used to understand the initiation treeing mechanism and improve the performance of power cable insulation.

Computational Methodology

A. SCCDFTB method

In the present study, all the electronic structure calculations and nonequilibrium quantum chemical molecular dynamics simulations were carried out by the self-consistent-charge density-functional tight-binding method including van der Waals correction (SCCDFTB-D)[22] with the DFTB+ program package.[23] DFTB is an approximate density functional theory method based on the tight binding approach, and utilizes an optimized minimal LCAO Slater-type all-valence basis set in combination with a two-center approximation for Hamiltonian matrix elements. The DFTB quantum chemical potential is ideally suited to bridge the gap between reactive force field approaches and first principles density functional theory (DFT) methods. It is several orders of magnitude faster than the latter but in contrast to the former it explicitly includes electronic effects.

All the nonequilibrium MD simulations in this study were performed based on a quantum chemistry method (QM), i.e. the self-consistent charge density functional tight-binding method. The nuclear equations of motion of nuclei were integrated using the Velocity Verlet algorithm[24] (Δt = 0.5 fs), and the nuclear temperature of 300 K with the NVT ensemble was maintained via a Nosé–Hoover chain thermostat.[25] To achieve convergence a finite electronic temperature approach[26] with T_e = 300 K was employed to evaluate the quantum chemical potential on the fly. Standard C-C, C-O, C-H, O-O, O-H, H-H, Si-C, Si-O, Si-H and Si-Si DFTB parameters were selected from the mio-0-1 set which are freely available at http://www.dftb.org.

B. IE, EA, and L.I. definitions

Electron affinity (EA) and ionization potential (IP) were commonly used to evaluated the charge injection abilities,[27-29] They were defined as follows,

$$EA_v = E_M - E_{M-//M} \quad (1)$$
$$IP_v = E_{M+//M} - E_M \quad (2)$$
$$EA_a = E_M - E_{M-} \quad (3)$$
$$IP_a = E_{M+} - E_M \quad (4)$$

where, the subscripts v and a represented vertical and adiabatic EA and IP. E_M, E_{M+}, and E_{M-} were the energies of neutral, cationic, and anionic molecules. $E_{M+//M}$ or $E_{M-//M}$ denoted the single point energies of cationic or anionic molecules based on the geometries of neutral molecules. Otherwise, the mobility of electrons and holes was also dominantly determined by reorganization energy λ.[30,31] A low λ value is necessary for an efficient charge transport process. Generally, reorganization energy is determined by the fast change of the molecular geometry when a charge is added to or removed from a molecule (the intramolecular reorganization energy λ_i) and slow variations in the surrounding medium due to the polarization effects (intermolecular reorganization energy λ_e). However, the previous reports[32,33] have demonstrated that λ_e is very small and λ_i is dominant in λ. Therefore, in the present study, we focus on the intramolecular reorganization energy λ_i, and the intramolecular reorganization energy for hole/electron transfer is simply defined as follows:

$$\lambda_{ih} = IP_v - HEP \quad (5)$$
$$\lambda_{ie} = EEP - EA_v \quad (6)$$

where, HEP or EEP represent hole or electron extraction potential, which were the energy difference between M (neutral molecule) and M+ (cationic), based on M+ geometry or the energy difference between M and M− (anionic), based on M− geometry.

The Lindemann index (L.I.)[34] was employed here to analyze the physical state and the mobility of polyethylene and SiO_2 nanocomposites, and it is defined as bellow,

$$\delta = \frac{1}{N(N-1)} \sum_{i<j} \frac{\sqrt{\langle r_{ij}^2 \rangle_T - \langle r_{ij} \rangle_T^2}}{\langle r_{ij} \rangle_T}$$

where N is the number of atoms in the relevant system, r_{ij} is the instantaneous distance between atoms i and j, and the brackets denote thermal averaging over a finite interval of time. The Lindemann index has been used on a number of occasions to elucidate the phase-transitions of transition metal and SiO_2 in the context of carbon nanotube or graphene nucleation and growth.[35-39]

C. Model

Regarding to the calculations of EA, IP, HEP, EEP, and λ, the nanocluster spheres with radius of 10 Å were prepared by cutting from the bulk structures, as shown in Fig. 1. The total numbers of the atoms (~400) were list in Table 1. In QM/MD simulations, three models were considered: (1) four molecules of $CH_3(CH_2)_{38}$-CH_3 with the density of 0.925 g/cm^3, depicted as PE_4, were set up in a periodic boundary box of 15.9×15.9×15.9 Å^3 according to the experimental conditions. (2) and (3) To save the simulation time and to provide the appropriate SiO_2 density, two SiO_2 spheres with the radius of 3 Å and 4.5 Å, which are almost the smallest nanoclusters of SiO_2, were

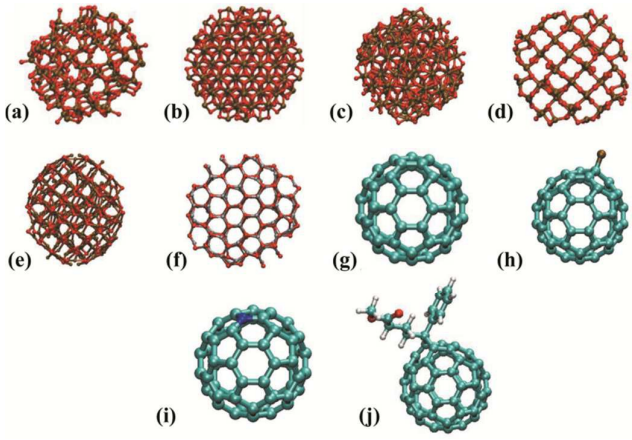

Fig. 1 The models of nanoparticles for IE and EA estimation. a) SiO_2; b) Al_2O_3; c) Fe_2O_3; d) TiO_2; e) CuO; f) ZnO; g) C_{60}; h) $C_{60}F$; i) $C_{59}N$; j) PCBM.

inserted into the above PE model. Thus, the SiO_2/PE nanocomposites ($C_{160}H_{328}Si_6O_8$ and $C_{160}H_{328}Si_9O_{22}$) with nanocluster content of 11.6 and 21.2 wt%, as model S and model L, were created. Since these two small nanoclusters are prepared by cutting sphere from the SiO_2 bulk, so they are not exactly with 1:2 stoichiometric ratios and therefore, in the discussion section SiO_2 is replaced by Si_xO_y to describe the interaction between SiO_2 and PE. The cubic periodic boundary boxes of 16.6×16.6×16.6 and 17.2×17.2×17.2 $Å^3$ were established to keep the constant density of 0.925 g/cm^3. To evaluate the trapping electron ability of nanocluster, the different number of electrons (from 1 to 4) were assumed in the two nanocomposite materials (S and L) and the pure PE systems, named as S^{n-}, L^{n-}, and PE^{n-} (n=1-4). Three independent trajectories with different initial velocities for each model were performed using randomized initial conditions. These trajectories were denoted as $\mathbf{S_m^{n-}}$, $\mathbf{L_m^{n-}}$, and $\mathbf{PE_m^{n-}}$ (m=1-3, and n=0-4).

Table 1 Ionization potentials (IP), electron affinities (EA), hole and electron extraction potentials (HEP and EEP), and internal reorganization energies (λ) (in eV) for the studied complexes. All the nanoparticles are cut as a sphere with the diameter of ~10 Å from the bulk.

	# of atoms	IP_v	EA_v	IP_a	EA_a	λ_{ih}	λ_{ie}	HEP	EEP
PE_4	488	7.14	-3.61	7.12	0.48	0.03	6.94	7.11	2.29
SiO_2	342	7.82	6.65	7.80	6.68	0.04	0.04	7.78	6.70
Al_2O_3	510	6.16	5.11	6.16	5.11	0.02	0.02	6.14	5.12
Fe_2O_3	418	2.17	1.17	2.16	1.19	0.02	0.02	2.15	1.20
TiO_2	404	4.02	2.92	3.99	2.94	0.05	0.04	3.97	2.96
CuO	418	5.00	3.97	4.99	3.98	0.02	0.02	4.98	3.99
ZnO	356	5.66	4.53	5.65	4.56	0.08	0.05	5.58	4.58
C_{60}	60	6.94 (7.60)[a]	2.95 (2.67)[b]	6.94	2.96	0.01	0.03	6.94	2.97
$C_{60}F$	61	6.85	3.38	6.83	3.41	0.04	0.07	6.81	3.45
$C_{59}N$	60	6.19	2.81	6.17	2.83	0.03	0.04	6.16	2.84
PCBM	88	6.66 (7.17)[c]	2.93 (2.63)[d]	6.59	2.97	0.10	0.07	6.54	3.00

[a-d] from ref. 22-25

Results and discussion

A. EA and IP

The IP[40] and EA[41] of the additives are correlated with the voltage stability, the electrical treeing, and dielectric strength of polymeric insulation materials. It has been proven that a high electron affinity of additives can increase the breakdown field by trapping of electrons to delay the formation of electron avalanche[42] and the breakdown strength of LDPE (low density polythylene) films.[43] Additionally, experimental and theoretical studies have already identified that high electron affinity and ionization energies were the necessary criteria for efficient electrical tree inhibition.[41,44] Therefore, in this study we calculated the vertical IP (IP_v), adiabatic IP (IP_a), vertical EA (EA_v), adiabatic EA (EA_a), as well as hole or electron extraction potentials and internal reorganization energies (HEP or EEP and λ_{ih} or λ_{ie}, which are related to the mobility of holes and electrons) of some additive nanoclusters investigated frequently in the experiments, such as, fullerenes and their devices (C_{60}, $C_{60}F$, $C_{59}N$, PCBM), and some other metal oxidizes (Al_2O_3, Fe_2O_3, TiO_2, CuO, ZnO). The values are listed in Table 1 and the investigated isolated nanocluster models are shown in Fig. 1. It is obviously that the calculated IP and EA values of C_{60} and PCBM are very close to the experimental data.[45-48] The IP is underestimated by ~0.6 eV and the EA is overestimated by 0.3 eV, which further confirm the validity of the DFTB method, while DFTB can extremely save the computational source and simulation time. We also found that the EA and IP values are ranging from 1.0~7.0 and 2.0~8.0 eV, respectively. It suggests that altering the nanoclusters is a possible way to tune the charge transfer properties for these complexes. Among all the investigated nanoclusters, it is obviously that SiO_2 possesses the largest IP, indicating that it is the most difficult hole injection materials. On the contrary, SiO_2 has the largest EA, which will contribute to a lower electron-injection barrier. Obviously, the introduction of an electron-injection nanocluster unit to the skeleton of PE would enhance their electron-injection ability. Our calculations indicate that SiO_2 is a promising candidate to reduce electrical treeing due to its high IP and EA. Regarding to the λ_{ih} and λ_{ie} all the nanoclusters hold the comparative values of ~0.05 eV, indicating the similar hole- and electron-transporting rate and excellent transfer balance. However, for PE, the λ_{ih} is extremely smaller than λ_{ie}, demonstrating the better hole-transporting performance for this complex. Since SiO_2 nanoclusters characterized a potential suppression electrical tree, QM/MD simulations were performed for these nano-filler composites.

B. PE Decomposition Mechanism on Si_xO_y Nanopaticles

We will initially discuss our QM/MD simulations on the interaction between Si_xO_y nanocluster and PE. Fig. 2 shows the optimized neutral structures of three models, PE^0, S^0, and L^0, respectively. Employing these optimized structures the 60 ps QM/MD simulations were performed. The final snapshots of all trajectories were provided as Supporting Information (Figures S1–S3). Since PE decompositions were similar, here we took four representative trajectories as the examples,

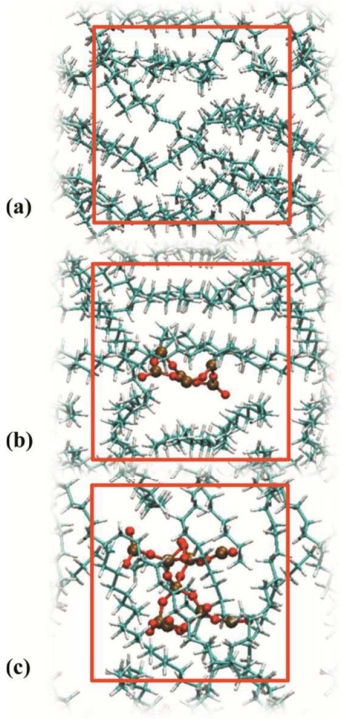

Fig. 2 The optimized geometries of three models. a) PE^0; b) S^0 (PE_4+SiO_2 nanoparticle with radius of 3.0 Å) and c) L^0 (PE_4+SiO_2 nanoparticle with radius of 4.5 Å).

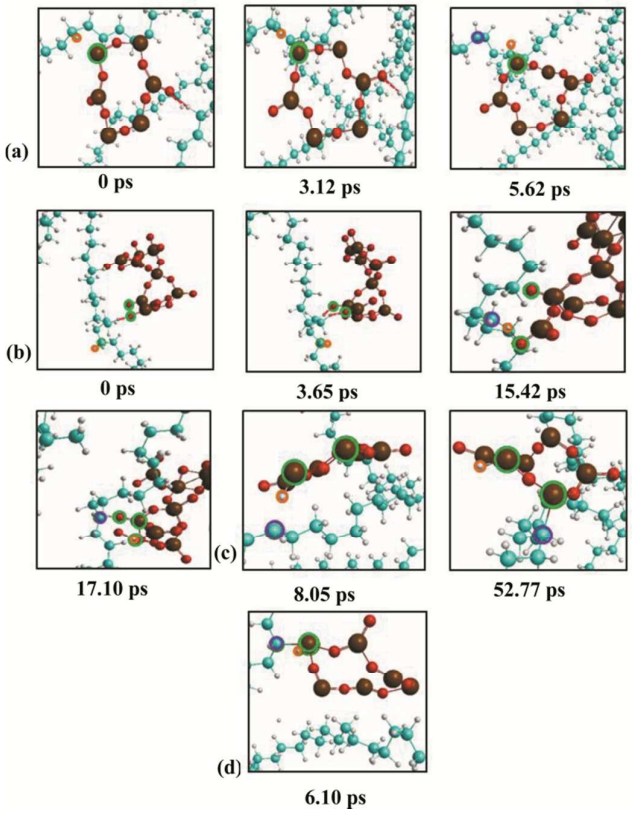

Fig. 3 The snapshots of H bond formation between H and O (red dashed line) or H transferring from polymer (CH_2) to nano-particle (Si or O), a) for trajectory 2 of model S^{2-}; b) for trajectory 3 of model L^0; c) for trajectory 1 of model S^{4-}; d) for trajectory 3 of model S^{4-}. The reactive H, Si, and C atoms are highlighted by orange, green, and purple circles.

shown in Fig. 3, to describe the PE decomposing process on Si_xO_y. Three typical procedures can be observed immediately from these figures. First, by the translational and vibrational diffusion of PE and nanocluster, the O…H hydrogen bonds (highlighted in red dashed line) were frequently formed and broken. Such as for S_2^{2-}, at 3.12 ps the O started to interact with the H in PE (Fig. 3a) and for L_3^0, at 3.65 ps two O gradually connected with two neighbor C-H to finally form a four-membered ring (Fig. 3b). These H bonds will lead to immobilized polymer interface[49] due to the strongly attraction of the polymer chains with the nanoclusters surfaces. Second, the H (highlighted in orange) transferring from polymer (-CH_2-) to nanocluster (Si or O) occurred and the -CH- radical was formed, which is the precursor for the branched structures. Although the hydrogen bonds were only observed between O and H due to the higher electronegativity of O and lower electronegativity of Si, both H transferring processes from polyethylene to Si and O took place. For example, for trajectories S_2^{2-}, S_1^{4-}, and S_3^{4-}, Si-H bonds were formed at 5.62, 8.05, and 6.10 ps, respectively. On the other hand, for L_3^0, O-H bond came into being at 15.42 ps, as seen in Fig. 3b. Third, Si-C or O-C bond was formed, as shown in Fig. 3, highlighted in purple (C) and green (O or Si). Followed H-abstraction reaction, the active -CH- radical was easily saturated by Si-C or O-C bonds. Two trajectories of S_1^{4-} and S_3^{4-} showed the Si-C formation and one trajectory of L_3^0 exhibited O-C formation at 52.77, 6.10, and 17.10 ps, respectively.

With regard to the PE decomposition process in pure PE, there was a dramatic difference to the nanocluster-filling composites. In pure PE model, with the number of trapping electrons increasing, the C-C bonds tended to broken which is, however, not observed in above nanocluster-filling composites. Fig. 4a depicts the C-C bonds broken procedure for $\mathbf{PE_1^{1-}}$($\mathbf{PE_2^{1-}}$ is similar to $\mathbf{PE_1^{1-}}$). During the 60 ps MD simulations, the C-C bond was continuous wobbling with C-C distance of ~2.3 Å, which was elongated by 53.3% compared to the C-C single bond. This C-C bond breaking/elongation was attributed to the repulsion of two negative charged carbon atoms (-0.41 and 0.40 e), as shown in red ball in Fig. 4b. It suggests that the C-C bonds were easily activated by the trapping electrons. Fig. 4c describes the averaged carbon cluster size at 60 ps. It was obviously that only for the pure PE system with one electron trapping (Model PE^{1-}), one C_{40} chain (totally four C_{40} chains) decomposed to C_{24} and C_{16} is observed. It is noted that for $\mathbf{PE_3^{1-}}$ the broken C-C bond was recovered during the 60 ps MD simulation, however, two C-H bonds were activated, as shown in Fig. 4a (right snapshot). The broken C-H bonds were elongated to 1.87 and 1.85 Å, resulting from the increased repulsive column interaction due to more negative charged carbon atoms (~-0.37 e). Consequently, in pure PE system, without the help of nanoclusters the redundant electrons were

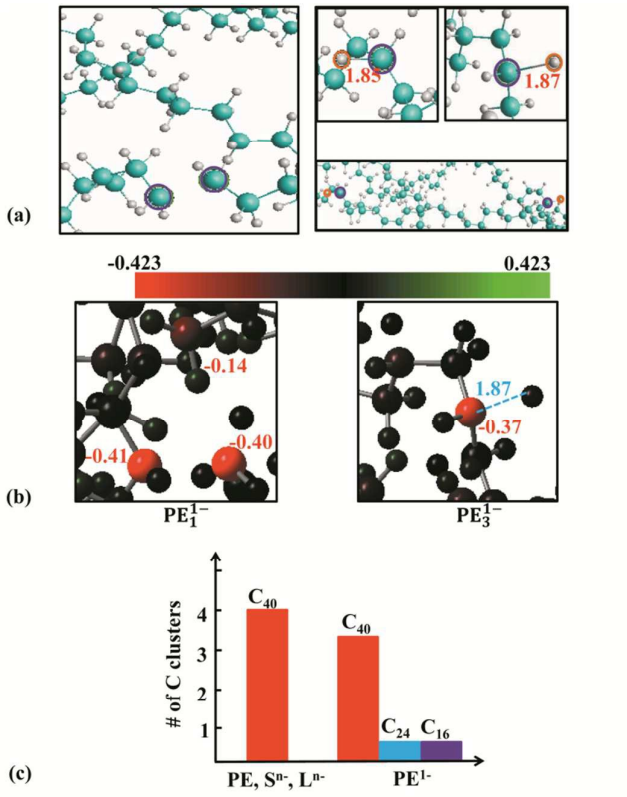

Fig. 4 The snapshots of C-C bond and C-H bond breaking in model PE. The left is for PE_1^{1-} and the right is for PE_3^{1-} (the up inset two figures are enlarged C-H broken structures); b) Mulliken charge distribution schematic of PE_1^{1-} and PE_3^{1-}; c) the averaged carbon cluster size at 60 ps, for all systems. The reactivated C and H atoms are highlighted by purple and orange circles.

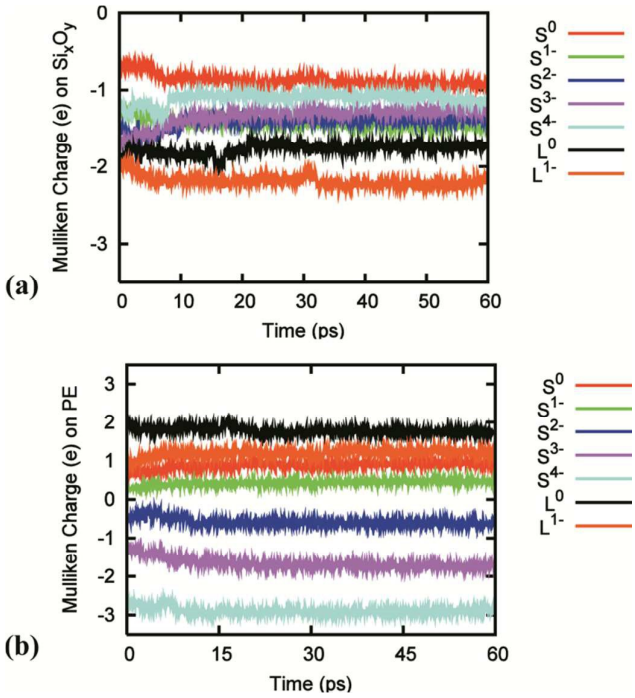

Fig. 5 The Mulliken charge as a function of time on, a) Si_xO_y nanoparticle and b) PE in small model with neutral (S^0), trapping one/two/three/four electrons (S^{1-}/ S^{2-}/ S^{3-}/ S^{4-}), and in the large model with neutral and one electron (L^0 and L^{1-}).

easily localized on certain carbon atoms and gave rise to the C-C and C-H bonds breaking. Contrarily, in the presence of the Si_xO_y nanoclusters, even trapping four electrons, there was still no C-C bond disruption and four C_{40} polyethylene chains were unchanged followed 60 ps MD simulations. It suggests that Si_xO_y filling can redistribute the electrons and prevent the C-C bond broken, to further reduce the initial precursor formation of electrical treeing and increase the tree initial time, in agreement to the experimental observation.[2-6]

C. Charge redistribution and Double Electric Layer

Obviously, the introduction of Si_xO_y nanoclusters redistributed the Mulliken charge, which attributed to the different electronegativity of C, H, Si, and O (2.55, 2.20, 3.44, and 1.90). Taking the average Mulliken charge analysis as an example, shown in Fig. 5, all Si_xO_y nanoclusters possessed negative charges from -2 to -1 depending on the different number of trapping electrons (from 0 to 4 e) and the size of filling Si_xO_y nanoclusters. With respect to the Mulliken charge on polyethylene chains (PE) in the nanocomposites (see Fig. 5b), when the nanocomposites were neutral and trapping one electron, PE in S or L model were always positive charged by 1 or 2 (red or black curve) and 0.5 or 1 e (green or orange curve). This promised PE can continuously accept electron-injection to reach stable neutral-close stage, and thereby a longer time was required for charge building up and delay the electrical treeing initial growth process, finally increase the tree initial time, which is consistent to the experimental observation.[2-5] Besides, it is clearly that the larger particle the more negative charge was located on the nanocluster (Fig. 5a S^0 VS. L^0 and S^{1-} VS. L^{1-}), suggesting that the ability of electrons trapping and collision was much dependent on the nanocluster size. The larger nanocluster or higher filler content led to more positive charged polyethylene, indicating that larger nanocluster or higher filler content can decrease the initiated rate of electrical tree more significantly, which agrees well with the experiment.[50] On the other hand, with the number of trapping electrons increasing from two to four, in S model, the polyethylene was gradually negative charged by -0.5, -1.5, -3 e, while they were still higher than the charge of pure PE system without nanocluster filling by 0.5~1 e. Therefore, the Si_xO_y nanoclusters can efficiently accumulate electrons and protect polyethylene from electrons trapping and collision. Furthermore, the behavior of Si_xO_y nanoclusters can largely decrease the energy of higher-energy electrons by trapping and colliding with them, thus, in some extent, the dielectric breakdown was relieved.

The interface behaviour between the nanoclusters and the polyethylene matrix is important in conductivity, permittivity, and the performance of space charge injection. Based on the interaction zones theory proposed by Lewis,[51] there exists an electric double layer around the nanocluster. In our simulations, we indeed observed the existence of the interface charges between nanoclusters and the polymers, as observed

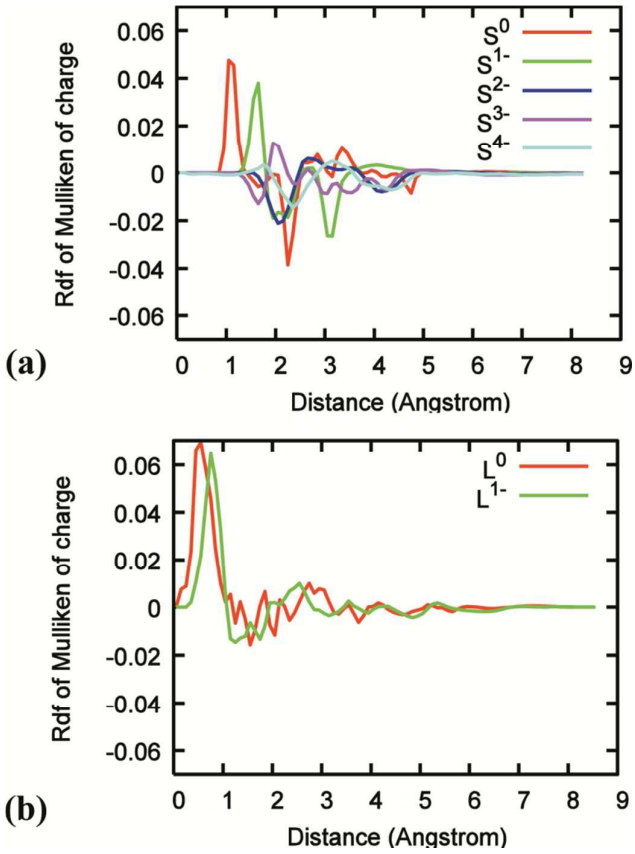

Fig. 6 The RDF of averaged Mulliken charge distribution around Si_xO_y nanoparticles from the mass center to radius of 8.5 Å. a) for Model S^{n-} (n=0, 1, 2, 3, 4); b) for Model L^{n-} (n=0, 1).

in the experiment.[52] Fig. 6a-b depicts the averaged RDF (Radial distribution function) of Mulliken charge distribution around Si_xO_y nanoclusters for Model S^{n-} (n=0, 1, 2, 3, 4) and L^{n-} (n=0,1), and the individual charge distribution for each trajectory are shown in Fig. S2. It is clearly that a multi-core model, proposed by Tanaka[53] was predicted here. A core-layer, a bound layer, and a free layer were observed in our SiO_2 filling composite. As we know that the nanocluster preferred to trapping electrons and consequently results in the redistribution of charge between nanocluster and the polymermatrix. From Fig. 6a we can see that for the neutral and trapping little amount charge systems (with negative charge of -1, and -2) the positive charge was distributed in the core-layer (1-2 Å from the mass center of SiO_2 nanocluster) and the negative charge was located in the out-layer at 2-3 Å. However, once the nanocomposite trapped too many electrons, such as with four electrons, there were two small positive charge layers available at ~1.8 and 3 Å, on the other hand, two larger negative charge layers were obviously observed with two peaks at 2 and 4 Å. This alternative positive and negative double electronic layer plays a very important role in explaining its impact on dielectric properties of polymeric insulations. Considering the size effect, the similarity is the positive core-layer is far away from the mass center with the number of trapped electrons increase. The difference is that the peak of core-level in L model was higher and closer to mass center than in S model, suggesting that the larger nanocluster the higher ability of trapping electrons, which is also consistent with the above Mulliken charge distribution and the experiment result.[50] We also found several separated small peaks for the large nanocluster system. We can deduce that there are large numbers of local charge domains distributed on the surface of the larger SiO_2 filling sample.

D. Mobility of polyethylene

Lindemann indexes (δ) for all systems are shown in Fig. 7 and Fig. S3. It is typically accepted that δ = 0.1 marks the transition between the solid and liquid phases.[54] Fig. 7 shows that polyethylene rapidly undergoes a solid to liquid-like phase transition upon thermal annealing, as indicated by the rapid increase of δ in all systems. Moreover, the increasing rate of pure PE from 10-60 ps was much faster than that of filling nanocluster systems (see Fig. 7a). It indicates that the mobility and the collision ratio were higher in pure PE system, making electrical treeing more easier initiated. On the contrary, the smaller δ for the Si_xO_y filling composite indicated a more solid-like character, which stabilized the polyethylene and impeded the chains collision. This immobilized interface agreed with the experimental result.[49] We also found that the number of trapped electrons can affect the mobility of polyethylene.

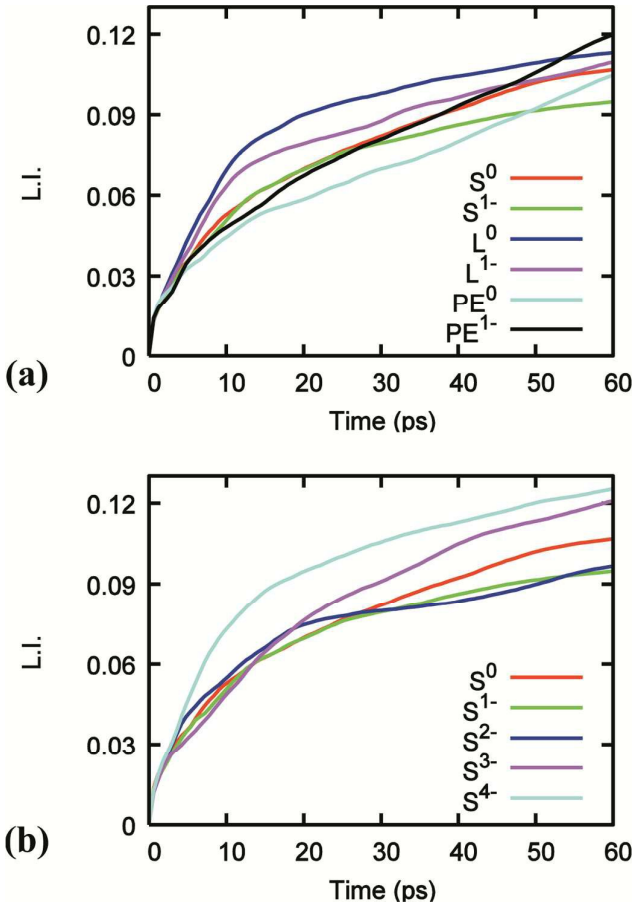

Fig. 7 The Lindman Index (L.I.) of CH atoms, a) for PE, S^{n-}, and L^{n-} (n=0, 1); b) for S^{n-}(n=0, 1, 2, 3, 4).

When the number of trapped electrons is small, for example one or two, the mobility restriction was more strongly with small value of δ. However, once more electrons were trapping into the systems, the mobility of polyethylene was increased, and δ was even larger than the pure PE systems. It indicates that the ability of trapping electrons or the immobilized polymer interface of Si_xO_y was only valid before "electron saturation". To get higher dielectric strength, the different size or various other nanoclusters should be characterized.

Conclusions

SiO_2 possessed the highest EA and was identified as one of efficient electron-injection materials. In our simulation, we summarized the role of SiO_2 as: First, SiO_2 can potently collide with the high energy electrons and decrease their energies due to the high electronegativity; Second, SiO_2 can efficiently trap the electrons, prevent the C-C bonds breaking, and further avoid the initial precursor growth of electrical treeing; Third, Si and O in the SiO_2 nanoclusters can interact with the H in PE by hydrogen bond, restricting the mobility of PE, which can stabilize PE and decrease the collision ability of PE chains, then keep from the initial branched structure growth to increase the tree initial time. In this paper, we observed the double electronic layer in the atomic scale, and we hope our observations are helpful to understand the electrical treeing mechanism and subsequently can be used in improving the properties of power cable insulation.

Acknowledgements

The authors thank National Science Foundation of China (grant No. 51337002, 21203174, 21221061, 21273219), Natural Science Foundation for Distinguished Young Scholars of Heilongjiang Province (JC201409), and the Natural Science Foundation of Jilin Province (Nos. 20130522141JH, 20150101012JC). The authors also thank the financial support from Department of Science and Technology of Sichuan Province. The computational resource is partly supported by the Performance Computing Center of Jilin University, China. We are also grateful to the Computing Center of Jilin Province for essential support.

Notes and references

1 K. Rajagopala, K. P. Vittal and L. Hemsingh, *J. Electr. Eng.*, 2012, **10**, 1904-1916.
2 R. Kurnianto, Y. Murakami, N. Hozumi and M. Nagao, *IEEE Trans. Dielectr. Electr. Insul.*, 2007, **14**, 427-435.
3 S. Alapati and M. J. Thomas, presented in part at the Fifteenth National Power Systems Conference (NPSC), IIT Bombay, 2008.
4 T. Iizuka and T. Tanaka, presented in part at the IEEE 9th International Conference on the Properties and Applications of Dielectric Materials, Harbin, July, 2009.
5 F. Guastavino, A. Dardano, E. Torello, M. Hoyos, J. M. Gomez-Elvira, P. Tiemblo and A. Ratto, presented in part at the Annual Report - Conference on Electrical Insulation and Dielectric Phenomena, Vancouver, BC, Oct., 2007.
6 M. Nagao, K. Oda, K. Nishioka, Y. Muramoto and N. Hozumi, presented in part at the Annual Report Conference on Electrical Insulation and Dielectric Phenomena, 2002.
7 M. Kawano, Y. Murakami, M. Nagao, Y. Sekiguchi, C. C. Reddy and Y. Murata, presented in part at the IEEE 9th International Conference on the Properties and Applications of Dielectric Materials, Harbin, July, 2009.
8 T. Tanaka, T. Iizuka, Y. Sekiguchi, Y. Murata and Y. Ohki, presented in part at the IEEE Conference on Electrical Insulation and Dielectric Phenomena, Virginia Beach, Oct., 2009.
9 Z. li, K. Okamoto, Y. Ohki and T. Tanaka, *IEEE Trans. Dielectr. Electr. Insul.*, 2011, **18**, 675-681.
10 H. Z. Ding and B. R. Varlow, presented in part at the Annual Report Conference on Electrical Insulation and Dielectric Phenomena, Oct., 2004.
11 A. Rashid, M. Ali and M. Asif, presented in part at the IEEE 13th International Multitopic Conference, Islamabad, Dec., 2009.
12 S. Alapati and M. J. Thomas, *IET Sci. Meas. Technol.*, 2012, **6**, 21-28.
13 D. Pitsa and M. G. Danikas, presented in part at the International Conference on Power and Energy Systems Dec., 2011.
14 T. D. Anthopoulos, B. Singh, N. Marjanovic, N. S. Sariciftci, A. Montaigne Ramil, H. Sitter, M. Cölle and D. M. de Leeuw, *Appl. Phys. Lett.*, 2006, **89**, 213504.
15 H. Li, B. C. K. Tee, J. J. Cha, Y. Cui, J. W. Chung, S. Y. Lee and Z. Bao, *J. Am. Chem. Soc.*, 2012, **134**, 2760-2765.
16 S. Rossbauer, C. Müller and T. D. Anthopoulos, *Adv. Funct. Mater.*, 2014, **24**, 7116-7124.
17 M. Jarvid, A. Johansson, R. Kroon, J. M. Bjuggren, H. Wutzel, V. Englund, S. Gubanski, M. R. Andersson and C. Müller, *Adv. Mater.*, 2015, **27**, 897-902.
18 P. H. Wöbkenberg, D. D. C. Bradley, D. Kronholm, J. C. Hummelen, D. M. de Leeuw, M. Cölle and T. D. Anthopoulos, *Synth. Met.*, 2008, **158**, 468-472.
19 M. H. Ahmad, N. Bashir, H. Ahmad, A. A. Abd Jamil and S. A.A., *TELKOMNIKA Indonesian Journal of Electrical Engineering* 2014, **12**, 5827-5846
20 K. Y. Lau and M. A. M. Piah, *Malaysian Polym. J.*, 2011, **6**, 58-69.
21 N. Shimizu, T. Takahashi and S. Iemura, presented in part at the IEEE 7th International Conference on Solid Dielectrics, Eindhoven, 2001.
22 M. Elstner, D. Porezag, G. Jungnickel, J. Elsner, M. Haugk, T. Frauenheim, S. Suhai and G. Seifert, *Phys. Rev. B*, 1998, **58**, 7260-7268.
23 B. Aradi, B. Hourahine and T. Frauenheim, *J. Phys. Chem. A*, 2007, **111**, 5678-5684.
24 W. C. Swope, H. C. Andersen, P. H. Berens and K. R. Wilson, *J. Chem. Phys.*, 1982, **76**, 637-649.
25 G. J. Martyna, M. L. Klein and M. Tuckerman, *J. Chem. Phys.*, 1992, **97**, 2635-2643.
26 R. M. Wentzcovitch, J. L. Martins and P. B. Allen, *Phys. Rev. B*, 1992, **45**, 11372-11374.
27 X.-N. Li, Z.-J. Wu, Z.-J. Si, H.-J. Zhang, L. Zhou and X.-J. Liu, *Inorg. Chem.*, 2009, **48**, 7740-7749.
28 L.-L. Shi, Y. Liao, G.-C. Yang, Z.-M. Su and S.-S. Zhao, *Inorg. Chem.*, 2008, **47**, 2347-2355.
29 Y. Liu, X. Sun, G. Gahungu, X. Qu, Y. Wang and Z. Wu, *J. Mater. Chem. C*, 2013, **1**, 3700-3709.
30 B. C. Lin, C. P. Cheng and Z. P. M. Lao, *J. Phys. Chem. A*, 2003, **107**, 5241-5251.
31 K. Sakanoue, M. Motoda, M. Sugimoto and S. Sakaki, *J. Phys. Chem. A*, 1999, **103**, 5551-5556.

32 X.-N. Li, Z.-J. Wu, Z.-J. Si, Z. Liang, X.-J. Liu and H.-J. Zhang, *Phys. Chem. Chem. Phys.*, 2009, **11**, 9687-9695.
33 X.-N. Li, Z.-J. Wu, X.-Y. Li, H.-J. Zhang and X.-J. Liu, *J. Comput. Chem.*, 2011, **32**, 1033-1042.
34 F. A. Lindemann, *Phys. Z.*, 1910, **11**, 609-612.
35 Y. Shibuta and T. Suzuki, *Chem. Phys. Lett.*, 2010, **498**, 323-327.
36 E. C. Neyts and A. Bogaerts, *J. Phys. Chem. C*, 2009, **113**, 2771-2776.
37 K. R. S. Chandrakumar, A. J. Page, S. Irle and K. Morokuma, *J. Phys. Chem. C*, 2013, **117**, 4238-4244.
38 A. J. Page, K. R. S. Chandrakumar, S. Irle and K. Morokuma, *Chem. Phys. Lett.*, 2011, **508**, 235-241.
39 A. J. Page, K. R. S. Chandrakumar, S. Irle and K. Morokuma, *J. Am. Chem. Soc.*, 2011, **133**, 621-628.
40 A. C. Ashcraft, R. M. Eichhorn and R. G. Shaw, presented in part at the IEEE Int. Symp. on Elec. Ins., 1976.
41 M. Jarvid, A. Johansson, V. Englund, A. Lundin, S. Gubanski, C. Muller and M. R. Andersson, *J. Mater. Chem. A*, 2015, **3**, 7273-7286.
42 E. Kuffel, W. S. Zaengl and J. Kuffel, Newnes, Oxford, UK, 2nd edn., 2000, ch. 5, pp. 281-366.
43 Y. Yamano, IEEE Trans. Dielectr. Electr. Insul., 2006, **13**, 773-781.
44 S. Kisin, J. den Doelder, R. F. Eaton and P. J. Caronia, *Polym. Degrad. Stab.*, 2009, **94**, 171-175.
45 B. W. Larson, J. B. Whitaker, X.-B. Wang, A. A. Popov, G. Rumbles, N. Kopidakis, S. H. Strauss and O. V. Boltalina, *J. Phys. Chem. C*, 2013, **117**, 14958-14964.
46 K. Akaike, K. Kanai, H. Yoshida, J. y. Tsutsumi, T. Nishi, N. Sato, Y. Ouchi and K. Seki, *J. Appl. Phys.*, 2008, **104**, 023710.
47 C. Brink, L. H. Andersen, P. Hvelplund, D. Mathur and J. D. Voldstad, *Chem. Phys. Lett.*, 1995, **233**, 52-56.
48 R. K. Yoo, B. Ruscic and J. Berkowitz, *J. Chem. Phys.*, 1992, **96**, 911-918.
49 L. A. S. d. A. Prado, *Plast. Res. Online.*, 2011, 1-2.
50 W. Yang, X. Yang, M. Xu, P. Luo and X. Cao, presented in part at the IEEE Conference on Electrical Insulation and Dielectric Phenomena (CEIDP), Oct., 2013.
51 T. J. Lewis, IEEE Trans. Dielectr. Electr. Insul., 2004, **11**, 739-753.
52 C. Zheng, W. Zhang, H. Zhao, X. Wang, Z. Sun and J. Yang, *IEEE Trans. Dielectr. Electr. Insul.*, 2014, **21**, 1493-1500.
53 T. Tanaka, M. Kozako, N. Fuse and Y. Ohki, *IEEE Trans. Dielectr. Electr. Insul.*, 2005, **12**, 669-681.
54 Y. Zhou, M. Karplus, K. D. Ball and R. S. Berry, *J. Chem. Phys.*, 2002, **116**, 2323-2329.

QM/MD simulations on the role of SiO_2 in polymeric insulation materials

Baozhong Han,[a] Menggai Jiao,[b] Chengcheng Zhang,[a] Chunyang Li,[a] Zhijian Wu,[b] Ying Wang*[b] and Hui Zhang*[a]

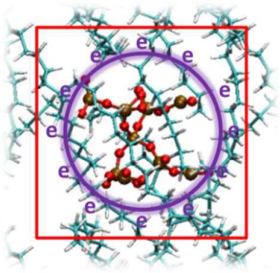

SiO_2 is one of the efficient electron-injection materials and can help stabilize polyethylene as in electric insulation material.